On the extension of the grain loop concept from 2D to 3D granular assemblies

Joao Chueire, Ali Daouadji, Francois Nicot, Antoine Wautier

On the extension of the grain loop concept from 2D to 3D granular assemblies

Joao Chueire[1,2*†], Ali Daouadji[1†], Francois Nicot[3,4†] and Antoine Wautier[5†]

[1*]INSA Lyon, GEOMAS, Lyon, France.
[2*]Ecole Centrale de Lyon, LTDS, Lyon, France.
[3] Grenoble Alps University, INRAE, UR ETNA, Grenoble, France.
[4] Savoie Mont-Blanc University, EDYTEM (USMB/CNRS), Bourget du Lac, France.
[5] Aix-Marseille University, INRAE, UMR RECOVER, Aix-en-Provence, France.

*Corresponding author(s). E-mail(s): jachueire@hotmail.com;
Contributing authors: ali.daouadji@insa-lyon.fr; francois.nicot@univ-smb.fr;
antoine.wautier@inrae.fr;
†These authors contributed equally to this work.

Abstract

In the field of granular materials, a link between the microscopic variables (contact force and displacement) and macroscopic variables (stress and strain) requires an intermediate scale called the mesoscopic scale. An important class of mesostructure is the so-called loops, which are closed chains of grains in contact. In two dimensions (2D), these structures tessellate a material domain into elementary partitions that account for the physics of granular materials. However, this property no longer applies in three dimensions (3D). In this paper, we propose to identify 3D mesostructures that generalize the 2D properties of loops and their ability to account for the deformability of granular materials. To do so, a weighted Delaunay Tessellation is used to partition a 3D specimen into tetrahedra. These tetrahedra are then merged through a criterion defined consistently with the one used to identify loops in 2D. As the 3D structures do not match the mathematical definition of loops, they are named clusters. A series of 3D DEM dry triaxial tests were performed to analyze the statistics of clusters during the loading path. It is shown that clusters behave analogously to loops, promoting an increase in the number of denser mesostructures during the strain contraction phase and looser ones during dilation. Furthermore, increasing amounts of looser clusters appear around force chains, promoting a decrease in the stability of the chained structures. Clusters are more diverse in shape and topology compared with loops. Thus, additional metrics besides the number of grains forming them are needed to characterize these structures. In this respect, we propose the concepts of order (number of external frontiers) and deformability.

Keywords: DEM, Granular materials, Mesostructures, Clusters, Loops, Delaunay tessellation, Force chains

1 Introduction

Granular materials are present in our everyday life and many industrial activities, taking many forms, from coffee grains to sand or snow. At first glance, these materials seem easy to understand since they

can be modeled as simple solids subjected to Newton's laws. However, due to the large number of particles, the variety of interactions and geometrical arrangements results in complex behaviors that have yet to be fully understood.

The emerging properties of granular materials can be analyzed at three different scales: microscopic, mesoscopic, and macroscopic. At the smallest one, the micro-scale, each grain behaves as a singular solid (often approximated as non-deformable) interacting with its neighbors through contact forces. At the macro scale, the whole specimen responds to loading stimulus as a continuum material for which the constitutive behavior results from a combination of the intergranular contact forces and geometrical properties. In between, the mesoscale provides a bridge between these two extremes and has attracted the interest of researchers over the last decades. At this scale, several mesostructures have been identified and studied as aggregates of attached grains or voids, such as loops [1–8], force chains [2, 3, 9–12] and pore structures [13–17]. These mesostructures account for both contact properties and local arrangements of grains and thus provide relevant clues to understanding the elementary mechanisms responsible for the macroscale properties of granular materials. In addition, loops statistics have been used to justify a constitutive model which uses elementary hexagonal patterns of adjoining particles to simulate the behavior of the granular media [18]. Considering mesostructures formed by a few grains allows the emergence of complex features at macroscopic scales, such as diffuse failure.

This paper focuses on a specific type of mesostructure, the so-called loops. They are formed by the branch vectors bridging convex grains in contact with each other [1]. In 2D, loops partition the material domain into elementary areas. Thus the sum of the volume of the loops is equal to the total volume of the specimen, the so-called pavement property. As a result, macro-scale properties can be upscaled as the surface-weighted average of loop properties. Based on the classical Love-Weber formula, several authors, [19–25], have shown that, under static or quasi-static conditions, a consistent definition of the stress tensor at that mesoscale can be derived through the weighted average of the tensorial product between the contact forces and the branch vectors of contacts into a given loop. Several approaches to derive the average strain tensors from geometrical quantities pertaining to loops and the relative displacements of each grain have been proposed [22, 26–31]. Kruyt et Rothenburg [4] used a loop tensor to identify their shape and orientation in relation to the principal load direction. Additionally, it has also been shown that the geometrical characteristics of loops influence force transmission in their neighborhood. For instance, loops composed of 3 grains are a vital source of stability and reinforcement of force chains (i.e. chains of highly stressed grains responsible for most of the force transmission within granular materials) [2, 3, 5]. As loops around force chains merge into larger structures, the probability of force chain bending events increases, possibly leading to the formation of shear bands (i.e. accumulation of strain in a narrow part of the specimen forming a band) [6, 11, 12, 32]. In fact, direct analysis of the local loop's distribution has shown that larger structures are more prevalent inside the shear bands in contrast with the rest of the specimen [33]. However, the use of loops to understand the behavior of granular materials has been limited to 2D conditions.

Over the past years, this dimension change has been regarded as a significant challenge [34]. Applying the definition of loops (as a minimal cycle in network science) to 3D conditions results in 2D structures incapable of partitioning a volume into sub-domains. Thus, identifying 3D mesostructures with comparable properties to 2D loops is not straightforward.

A different way of partitioning granular materials starts from characterizing the granular void space, the so-called pore structure [14, 17, 35–40]. For instance, the assembly can be described as a set of large voids (pores) interconnected by smaller voids (constrictions) in 2D and 3D conditions [34]. After the work by Mellor [41], the Delaunay tessellation has been widely used in many pore-space definitions. Using the grain's centers as seeds, the tessellation divides the entire specimen into tetrahedra (or triangles in 2D), partitioning the media. These elementary structures are then joined through a merging criterion to create the pore space [14, 17, 35–40].

However, the pore structure's criterion is not fully adapted to study contact-based mesostructures, as illustrated in Figure 1, where two pores are created for a single loop. Indeed, the two classes of mesostructures aim to characterize different physical phenomena: the transport properties in the void space for pores and the volumetric behavior of the material for loops.

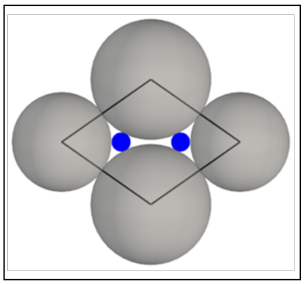

Fig. 1 Example of a loop containing two distinct pores, each represented by a blue sphere.

In this paper, we propose using the Delaunay tessellation to transpose the 2D definition of loops to 3D conditions, thus introducing 3D loop-like structures. As we are interested in a contact network between grains, an early definition based on grain's contacts, proposed by Nguyen et al. [34], will be considered and extended. This will provide a framework to quantify mesoscale deformability properties.

The paper is organized as follows. First, the definition of loops in 2D conditions through a Delaunay tessellation is briefly reviewed. Then the 3D extension of this process is proposed. Next, the numerical experiment used to validate the approach is described in detail. Then we demonstrate that the 3D loop-like concept presented in this paper can be regarded as a relevant 3D counterpart of loops that conveys much of the volumetric properties of granular materials.

2 From 2D Loops to 3D Clusters based on a Delaunay tessellation.

In this paper, the elementary shapes created by the Delaunay tessellation will be referred to as cells, while the connections formed between the grain's centers will be known as edges. This is illustrated in Figure 2, where a 2D example is shown.

To identify loop structures, specific cells must be merged. A relevant merging criterion must be related to the contact network and its ability to deform.

2.1 Review of the 2D definition of loops

The Delaunay tessellation connects pairs of grains through edges regardless of physical contact. Hence two categories of edges arise: closed and open. Closed edges are defined as those in which the connected grains are in physical contact, while open edges correspond to connections between grains not in contact.

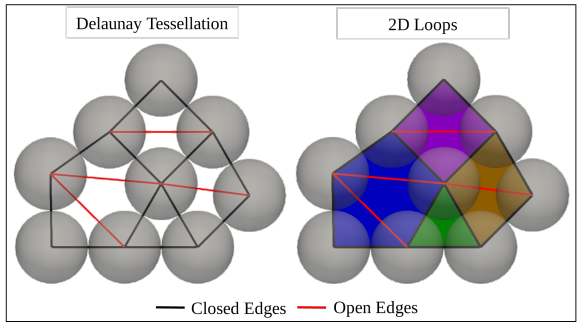

Fig. 2 Identification of loops through Delaunay tessellation

The loop structure is formed by a group of grains in contact enclosing a common void space. In other words, it is equivalent to polygons composed of only closed edges on their boundaries. As each edge is the frontier between exactly two cells, a convenient merging criterion involves joining adjacent cells sharing a common open edge. Thus, the merging criterion can be defined as the presence of an open frontier between two distinct cells. This procedure is illustrated in Figure 2.

2.2 Generalizing the 2D algorithm to 3D conditions

In 3D, each cell of the Delaunay tessellation is a triangular-based pyramid composed of four surfaces and six edges, as illustrated in Figure 3.

In 3D, the frontier between two cells is a triangular surface. However, the definition of an open

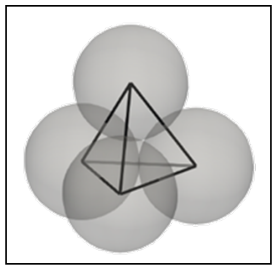

Fig. 3 Example of a 3D cell.

or closed frontier in 3D is not as straightforward as in the previous case. Indeed, four configurations can be derived from the combination of open and closed edges.

Nguyen et al. [34] considered that the presence of an open edge defines a 3D open frontier. However, as each edge is shared by several 3D cells, this criteria results in the incorporation of all the cells around each open edge into a single structure. Furthermore, even for dense specimens, most edges generated by the tessellation are open, as illustrated by figure 4. Thus, this definition detects an enormous structure containing most cells within the considered specimen (70%) [34]. This proposition is, therefore, not restrictive enough to avoid merging a disproportionate number of tetrahedra.

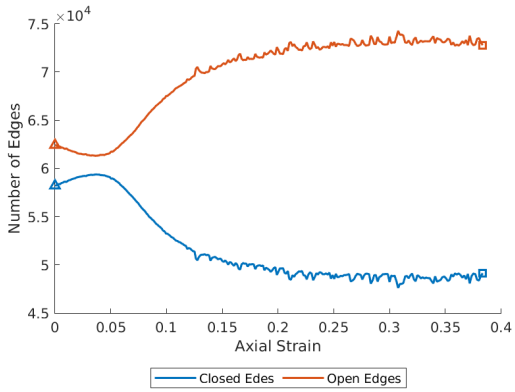

Fig. 4 Open and closed edges distribution for a dry triaxial test with confining pressure of 100kPa (Test D100).

We propose in the present paper that an open frontier exists in 3D only when all its edges are open. As a result, a closed frontier corresponds to all other cases where at least one edge is closed, as illustrated in Figure 5.

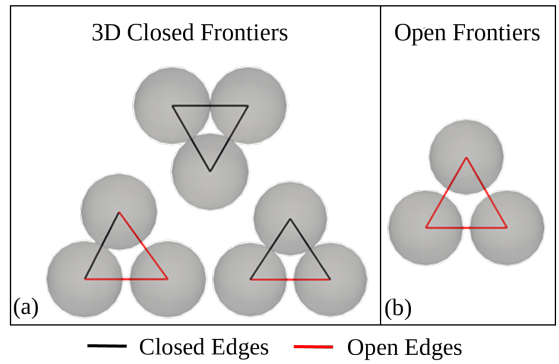

Fig. 5 Example of closed (a) and open (b) frontier in 3D.

With the frontier's categories thus defined, the 2D loop detection algorithm can be extended to 3D conditions. Figure 6 illustrates the creation of a 3D mesostructure by joining two cells.

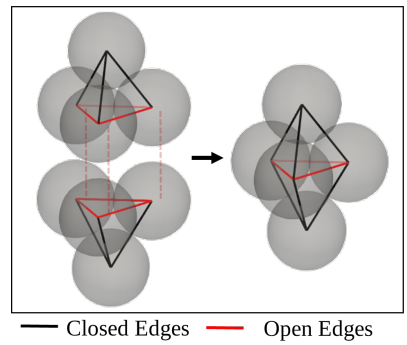

Fig. 6 Merging two cells to create a cluster of order 6.

The loop structure defined in section 2.1 can be seen, in a mathematical framework, as a chain of edges in which no vertex besides the first appears more than once. Thus, in 2D, a bijection exists between a polygon and the loop composed of its vertices. However, in 3D, it is impossible to cycle through a structure's grains and edges without repeating elements. Therefore, the word loop is not adapted to the 3D framework, and subsequently, these structures will be called clusters. In the following, "loop" refers to contact-based structures in 2D conditions, while "cluster" refers to their 3D counterpart.

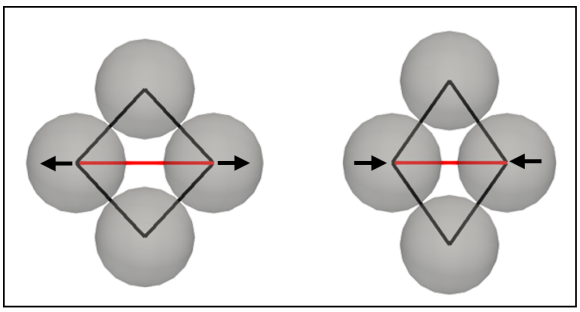

Fig. 7 Possible configurations for a loop of size 4, in 2D.

2.3 Size and Order

The classical way to categorize a loop corresponds to the number of grains or exterior frontiers forming the structure [2, 7, 33], generally referred to as size or order. For loops, these two quantities are equal. However, this is no longer true in 3D conditions, where both metrics are necessary to describe clusters. Thus, an extension of the meaning of these terms is proposed: size defines the number of grains forming a structure, while order refers to the number of external frontiers.

The order of a loop or cluster can be directly obtained from the number of cells and open frontiers of the structure. It is accounted as the difference between the total number of frontiers and the number of open ones, as shown in Eq.(1).

$$O = (d+1)N_{Cells} - 2N_{OpenFrontiers} \quad (1)$$

With d being the number of dimensions (2D or 3D), N_{Cells} the number of cells, and $N_{OpenFrontiers}$ the number of open frontiers.

Alternatively, a universal relation between size, cells, and open frontiers cannot be achieved. In the following, the order metric will be favored for the overall analysis of cluster statistics.

2.4 Deformability of clusters

The local characteristics of the contact network influence how deformable the granular assembly is. For instance, a loop of order 4 or greater can adopt several possible configurations to accommodate the displacement of grains, as illustrated by Figure 7.

The analysis of the configurational entropy of a structure has been shown to be capable of measuring the degrees of freedom of loops [7, 42]. However, the definition of this property for loops or clusters is not simple and would require a paper of its own. In particular, the definition of the set of admissible configurations and their related probability of occurrence. Thus, deformability is introduced here as a simple but efficient metric to quantify the degree of interconnectivity between a cluster's grains according to their topological characteristics.

The feature that allows a loop to adopt more configurations and thus to be more deformable is the presence of open edges. The deformability of a loop is then proposed as the ratio between the number of open edges and total edges, as shown in Eq.2:

$$D = \frac{N_{OpenEdges}}{N_{TotalEdges}} \quad (2)$$

As the number of edges is directly related to the order of a loop, Eq.2 can be rewritten in 2D conditions as follows:

$$D_{Loop} = \frac{O_{Loop} - 3}{2O_{Loop} - 3} \quad (3)$$

With O_{loop} being the loop order, a nondeformable loop of order 3 has a null deformability value. The deformability increases with the loop order, with a maximal possible value approaching 0.5 for impossibly large loops.

Eq.2 can be directly applied to 3D conditions. Even though edges are no longer the frontier between cells, they still account for the connections between grains. Thus, the presence of open edges is still the necessary condition for a cluster to be deformable. However, as shown in Figure 5, 3D frontiers are created from different configurations of closed and open edges. Hence, an equation equivalent to Eq.3 cannot be derived for 3D conditions, and no simple relation between the deformability and the order of a cluster exists. Consequently, two clusters created with the same set of grains, order, and size may have different values for the deformability, further highlighting the jump in complexity when moving from 2D to 3D.

2.5 Clusters Search Algorithm

Using the merging criterion defined in sections 2.1 and 2.2, an algorithm was designed to find clusters and loops inside a granular assembly. The

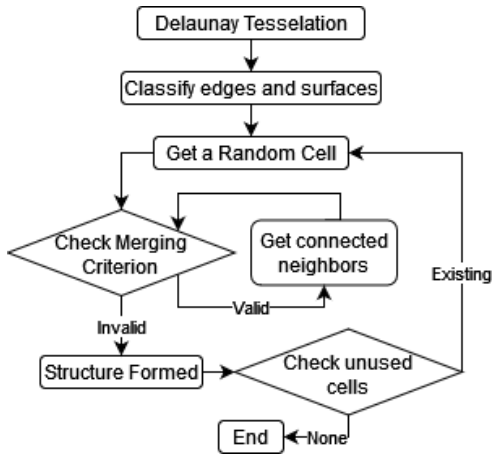

Fig. 8 Cluster search algorithm flowchart.

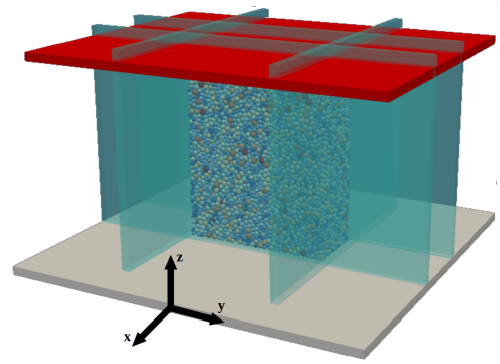

Fig. 9 Model illustration. The vertical piston is represented in red (z-axis), the fixed base is represented in gray, and the four horizontal pistons are represented in a transparent blue (x-y plane).

algorithm, summarized in the flowchart given in Figure 8, is mainly composed of the three following steps :

- Use a Delaunay Tessellation with the grains center's position as seeds to obtain a cell system to feed the algorithm. For polydisperse distribution, a weighted Delaunay tessellation is recommended.
- Using the grain's physical contact network, categorize the frontiers between adjacent cells as open or closed.
- A seed cell is randomly selected. Then the merging criterion is recursively checked, merging valid adjacent cells. When the merging criterion is no longer applicable, the final mesostructure is returned, and a new seed cell that has not yet been merged is selected.

It should be stressed here that the algorithm is deterministic since the Delaunay tessellation is unique (except in rare pathological cases where centers of 4 grains lie on a common sphere). This uniqueness property is essential for the temporal evolution of clusters from one state to another.

3 DEM Triaxial Simulations

A numerical model was created to test the detection algorithm using the Discrete Element Method (DEM) software LIGGGHTS [43]. Data from the simulation is post-processed with MATLAB to extract the data presented in the following sections.

The simulation setup consists of a prismatic box measuring $0.15 \times 0.35 \times 0.45$ m^3 with a fixed base at the bottom and five pistons in all other directions, as illustrated in Figure 9. The contact model uses Hertz contact law with a Coulomb friction limit and a damping force calculated through a restitution coefficient. The normal and tangential spring stiffnesses (k_n and k_t) are directly calculated by LIGGGHTS as a function of the interpenetration between two grains and the chosen material parameters reported in Table 1. Additionally, a third spring is used to insert artificial rotational friction into each particle, introducing a new spring stiffness (k_r) calculated as a function of the normal and tangential stiffnesses.

The specimen is created through gravity deposition. Next, all pistons are activated to apply a targeted isotropic pressure. After the equilibrium is reached, the vertical piston control is changed to impose a constant compression speed of around 2 mm/s while the stress of the lateral pistons is kept constant. This is known as a drained triaxial test in the field of geomechanics. The sample is vertically compressed until the vertical axial strain reaches around 38%. As no liquid is included in the model, total and effective stresses are equal.

Three different numerical experiments were conducted with varying isotropic pressures (50 kPa, 100 kPa, 200 kPa) departing from the same cloud of grains. The tests are labeled D50, D100, and D200, respectively. The interval between measure points was chosen at 2.5 s (12,500 calculation steps), corresponding to a displacement of the vertical piston of 5 mm.

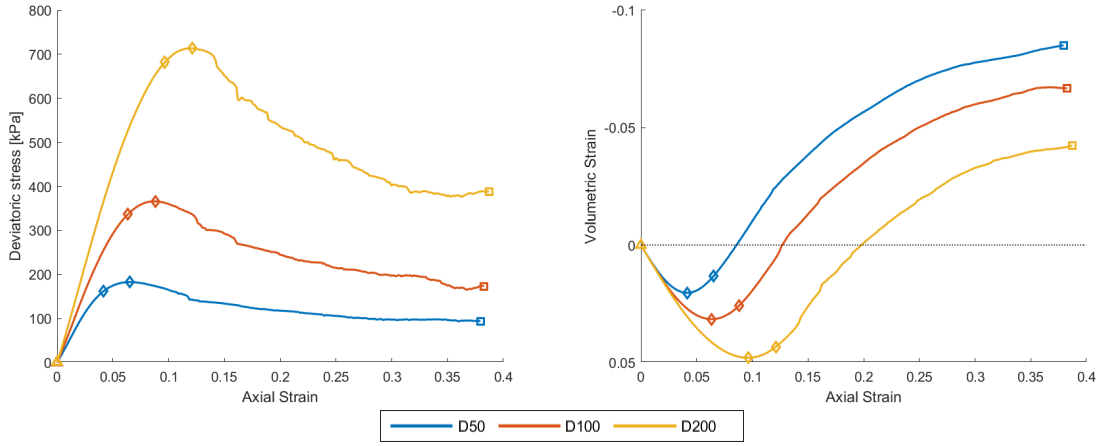

Fig. 10 Evolution of the deviatoric stress (left) and volumetric strain (right) with respect to the axial strain. Continuum mechanics convention is used with positive dilation. The triangle and square symbols indicate the start and end of the test, respectively, while the diamond is the characteristic point and the circle the peak deviatoric stress.

Table 1 Material information for DEM simulation.

Dimensions	$0.15 \times 0.35 \times 0.45$ m^3
Elastic modulus	10^8 Pa
Stiffness ratio	0.25
Friction coefficient	0.57
Wall friction coefficient	0.00
Rolling friction coefficient	0.30
Restitution coefficient	0.50
Number of particles	19.136
Particle diameter	8 to 16 mm

Figure 10 shows the macroscopic mechanical response of the three specimens, where the volumetric strain and the deviatoric stress are plotted against the axial strain. The stress was calculated using the standard Love-Webber formula [19, 20, 44–46], and the strain was calculated using the pistons displacement data in a Lagrangian framework.

The sample's mechanical response is illustrative of dense granular materials with a stress hardening followed by softening and a contractive then dilative strain behavior. Between these regime changes, three regions are highlighted and identified by different marks in Figure 10:

- From the beginning (triangle mark) until the characteristic point (diamond mark), the specimen is in contraction and hardening regime.
- After the characteristic point (diamond mark), the total volume increases. Thus, until the peak deviatoric stress (circle mark), the specimen is in a dilation and hardening regime.
- After the peak deviatoric stress (circle mark), the strength of the specimen decreases, characterizing the change to dilation and softening regime.

To ease the correspondence between the meso and macro behaviors, the four marks used in Figure 10 will be shown systematically in all upcoming curves: a triangle at the beginning of the test, a square at the end, a diamond at the characteristic point (change from compression to dilation) and a circle at the peak deviatoric stress (change from hardening to softening).

4 Clusters Statistics

Figure 11 illustrates a few clusters of different orders and sizes, their different geometrical configurations, and their location in the specimen. These structures can be seen to adopt different forms, from more elongated ones like cluster A (Order 70) or more clumped ones like cluster C (Order 72). It is also worth noting the difference between the order and size of these two clusters, as cluster A has a larger size than cluster C but a smaller order. I

Clusters exhibit a wider variety of orders compared to their 2D counterpart, as illustrated in Figure 12 containing the evolution of the maximal order of clusters during the numerical tests.

Two stages can be identified, coinciding with the contraction and dilation regimes. In the early stage, the maximal order remains stable. Later,

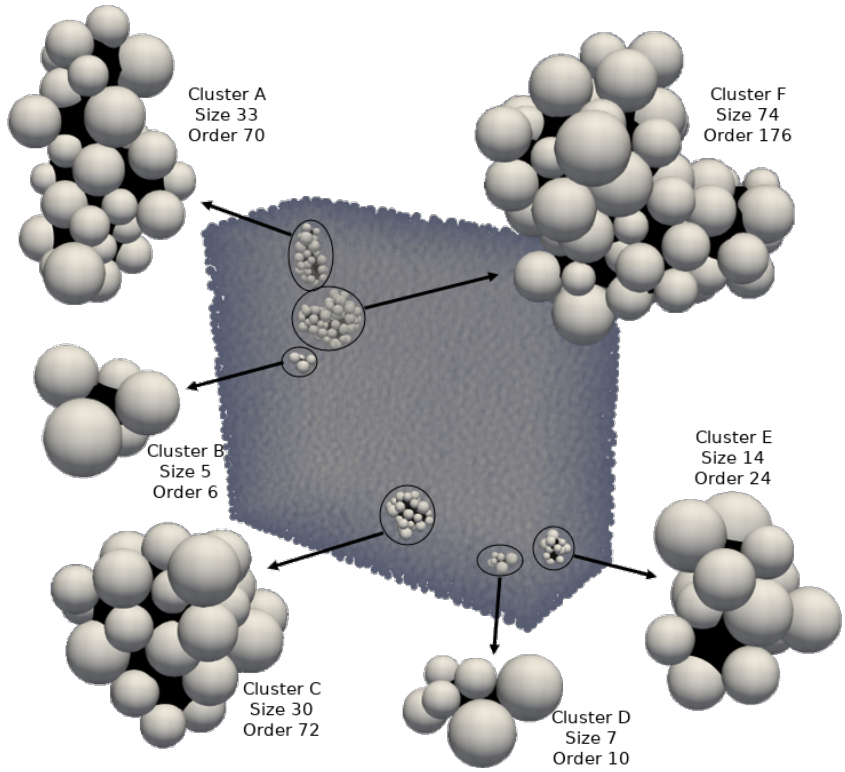

Fig. 11 Examples of clusters of various forms and positions inside a prismatic specimen.

when dilation is installed, clusters of larger order appear, peaking around the order of 250 in the test D100.

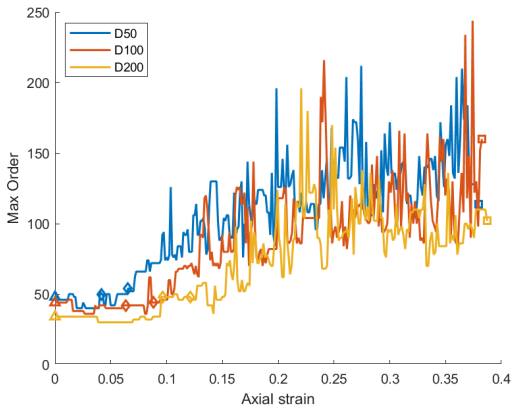

Fig. 12 Evolution of the maximal cluster order for the three confining pressures used in the dry triaxial tests.

Because of the wide range of cluster orders in 3D, the study of their distribution requires the definition of categories. These were defined considering their behavior regarding being created or destroyed in relation to the axial strain, as illustrated in Figure 13. The clusters can be described in the following four categories:

1. *Small - Order 4.* This category is by far the most numerous. This cluster population increases during the contraction phase but decreases when approaching the dilation regime until a constant value is reached.
2. *Submedium - Order 6.* In the early stages, this population evolves opposite to small clusters, decreasing during the contraction and increasing during the dilation. However, near the deviatoric stress peak, submedium clusters decrease until a steady state is reached.
3. *Medium - Order 8 to 20.* The population of medium clusters evolves similarly to submedium ones until the peak deviatoric stress, from where it keeps growing until a steady state is reached. In fact, medium and small cluster populations evolve in opposite ways.

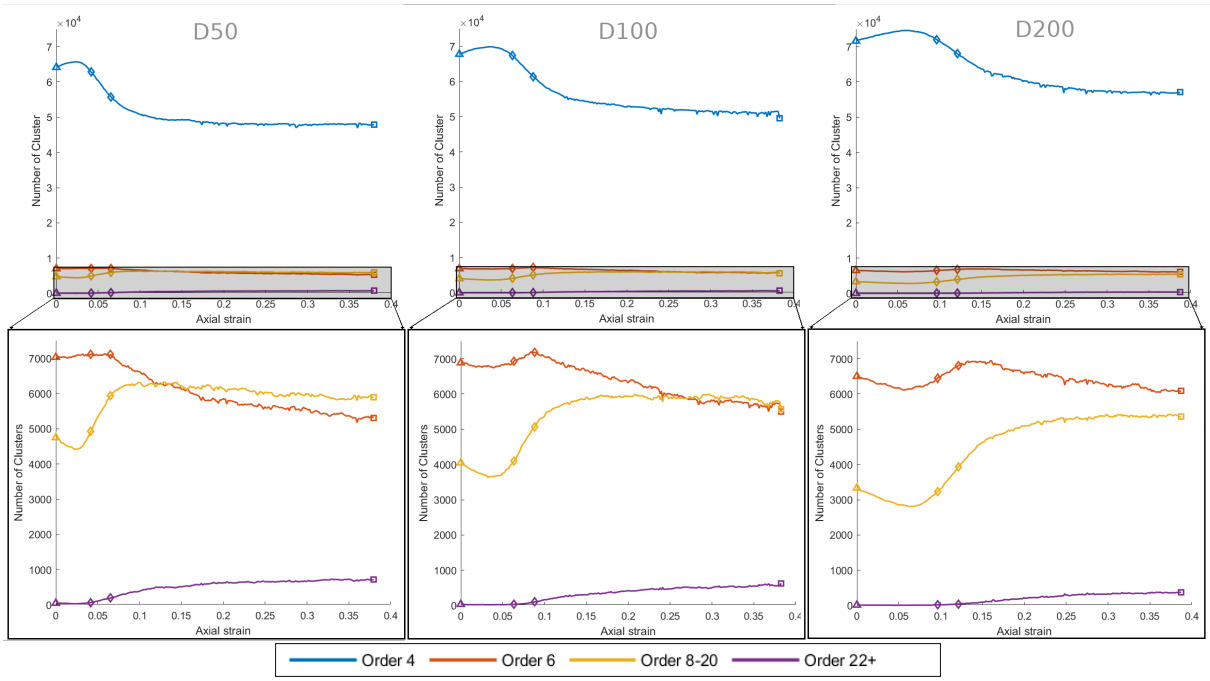

Fig. 13 Evolution of clusters categories over the loading path. Each plot represents a constant confining stress of 50 kPa (D5O), 100 kPa (D100), and 200 kPa (D200), respectively. The second row is a zoom of the first.

4. *Large - Order 22+*. This category of clusters encompasses all clusters larger than the medium category [1]. They appear in significant amounts after the characteristic point, growing in number until a constant value is reached at large vertical strains.

The overall behavior of each cluster category remains qualitatively similar between the three simulations. In the early stages, the samples are in a contraction regime. Therefore, the particles are being reorganized within the specimen, destroying structures of high void ratio and forming denser ones. In other words, medium and submedium clusters are broken to create small ones.

However, this trend reverses when the volumetric strain rate starts to decrease. Clusters start merging, thus reducing the number of small clusters and creating structures of all other categories. As increasingly larger structures start to appear, the specimen dilates.

Next, near the deviatoric stress peak (circle mark), submedium clusters start decreasing in number, thus diverging from the behavior of the medium category. Not long after, small and medium clusters stabilize in number, while clusters of submedium and large categories reach an asymptotic value at large strains when approaching the steady state.

The deformability data of all clusters observed in the three tests are scattered in Figure 14. The black curve represents the average deformability for each cluster order, while both blue curves are fittings of the maximal and minimal values per order.

It can be noted that the average deformability value increases with the order of the cluster, stabilizing for high orders. The average deformability value observed for the minimal cluster is around *0.49*, indicating that most of these clusters are indeed deformable, in contrast with the non-deformable 2D counterpart (deformability equal to 0).

In addition, the blue curve in figure 14 marking the upper boundary of the observed deformability values is almost a straight line. This indicates that clusters may have a maximum deformability value

[1] The limit between medium and large categories is defined by the largest cluster existing from the beginning of the test in significant amounts. Other initial conditions (like a looser soil) might be useful to precise which order is the most relevant to distinguish medium and large cluster groups.

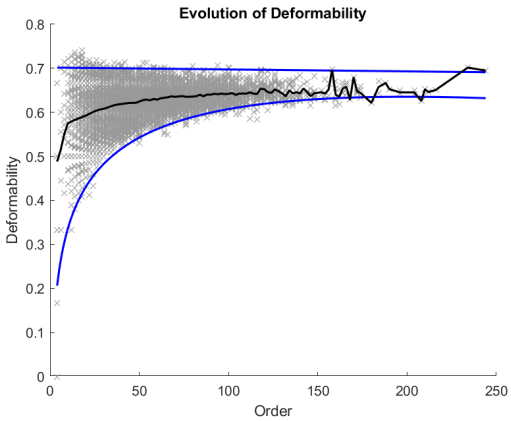

Fig. 14 Deformability distribution of all clusters identified in the three tests with respect to the cluster order. The black curve represents the mean deformability per order, while the blue curves are fittings of the minimal and maximal values.

of around *0.7* for large orders. Thus, it could be inferred that a minimum of approximately *30%* of closed edges are required to form a cluster.

The dispersion of values is much more prevalent for clusters of a smaller order. In fact, it can be shown that the minimal deformability value increases with the order of a cluster, as an increasingly higher proportion of open edges is necessary to form them. Consequently, the deformability is bounded by an increasingly smaller interval with increased order.

Small clusters (of lower deformability) are more prevalent in the early stages, resulting in a sturdier structure. However, as larger and more deformable clusters appear, the specimen loses strength and becomes more deformable.

The behavior of cluster categories can be compared to the results of dense soil under drained biaxial conditions in 2D found by Zhu et al. [12]. Figure 4 in [12] shows that loops of order 3 are created during the contraction phase, while loops of order 6+ are destroyed. Later, when the dilation regime is installed, the behavior reverses, and the formation loops of order 6+ are now promoted. The creation and destruction of loops primarily affect these two categories, while the others remain nearly constant. Small clusters behave analogously to loops of order 4, while large clusters are related to loops of order 6.

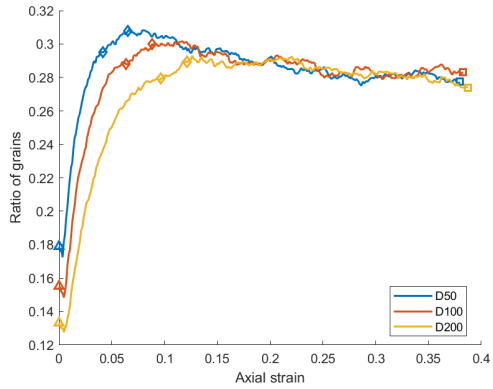

Fig. 15 Evolution of the fraction of grains belonging to force chains.

5 Clusters and Force Chains

It has been previously shown, in a 2D framework, that force chains and loops have a close relation [2, 3, 12]. Force chains start to bend and buckle when contacts in their neighborhood are lost, corresponding to an increase in local deformability. From the point of view of loops, their order around force chains increases.

To highlight this property in 3D conditions, force chains were identified through the procedure proposed by Peters et al. [10]. Figure 15 illustrates the evolution of the fraction of grains involved in force chains, known as chained grains.

In the early stages, the ratio of chained grains grows rapidly, consistent with the macroscopic hardening of the specimen. Later, a peak value is reached, followed by a decline in chained grains. As force chains are no longer being created, the existing force chains become overloaded and start bending/buckling to accommodate external stimulus, thus resulting in a softening phase.

The cluster populations can be subdivided into force chain clusters (FCC) and non-force chain clusters (NFCC). An FCC is a cluster that actively participates in force transmission. As the contact between grains defines force chains, a cluster will be considered FCC if at least one of its closed edges is part of a force chain. In opposition, an NFCC is a cluster without a common edge with a force chain and thus does not participate actively in the force transmission.

The distribution of cluster categories for FCC and NFCC populations is illustrated in Figure 16

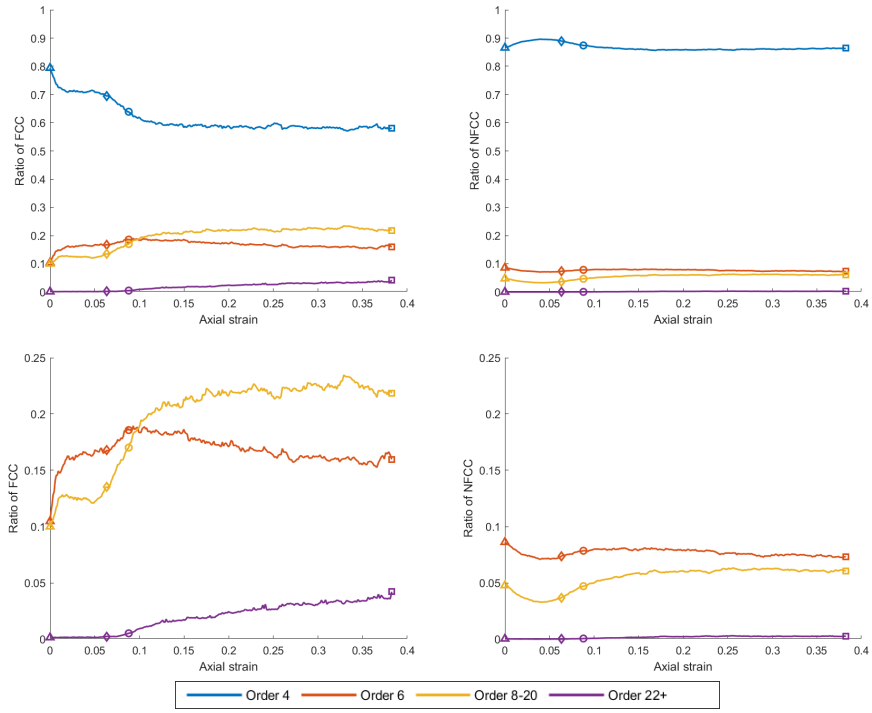

Fig. 16 Cluster categories distribution on two domains for the test D100. Left force chain clusters (FCC) and right non-force chain clusters (NFCC). The second line of figures is a zoom of the first in the higher categories of clusters.

for the test D100. Similar results were obtained for the tests D50 and D200 (not shown here).

A clear disparity between FCC and NFCC can be observed during the loading path. At any stage of the test, the amount of submedium, medium and large FCC is superior to NFCC, indicating a preference for larger clusters to be around force chains.

At the very early stages, a rapid transition between categories is observed as the specimen adapts to the vertical load. Then, a region with few transitions between cluster categories was observed before the characteristic point. During this stage, many grains are recruited inside force chains. It can be concluded that the newly formed force chains are well distributed in the specimen, maintaining the FCC and NFCC proportions.

However, around the characteristic point, clusters start merging, increasing the proportion of all categories besides the small one. It can be noted that the transitions between categories are more representative for FCC. This indicates that a substantial amount of grain rearrangement occurs around force chains, thus increasing the average order of FCC. In addition, as increasingly larger FCC are formed, the stability of the force chains decreases, thus preparing the subsequent force chain bending (and buckling) phase leading to the softening regime.

This section's results can be compared to the analysis of the relation between loops and force chains done by Zhu et al. [12]. Figure 7 of the mentioned article compares force chain loops (FCL) and non-force chain loops (NFCL). An apparent disparity between the number of loops of both groups can be observed. The amount of FCL of higher orders is superior to NFCL. In addition, the transitions between FCL categories were more prevalent, with increasing amounts of FCL of order 6+ being created.

Finally, these results confirm the importance of loops and clusters for the macroscopic behavior of granular materials in both 2D and 3D conditions. The transition rate between loops or cluster categories is reflected macroscopically as volumetric strain rate fluctuations. Furthermore, the presence of structures of higher deformability around force chains decreases their stability, thus impacting the stress state of the specimen.

6 Concluding Remarks

This paper proposed a definition of clusters as 3D structures equivalent to 2D loops for granular assemblies. A Delaunay tessellation was used to subdivide the sample into small tetrahedra called herein cells. Each cell comprises edges and triangular surfaces classified into open and closed groups. A surface is considered open if all three edges forming it are open. A cluster is formed by joining cells sharing a common open surface, thus defining a merging criterion. This definition was then validated by a series of DEM simulations of dry triaxial loading tests with a dense specimen, which proved that the newfound structures behave analogously to their 2D counterparts regarding overall evolution and behavior around force chains.

It was shown that the cluster's evolution directly correlates with the macroscopic behavior of the specimen. At the early stages, small clusters, which are more stable, increase in number, resulting in the contraction of the sample. Later, grain reorganization forces small clusters to merge, creating increasingly larger structures. Thus, the macroscopic strain rate decreases, ultimately leading to dilation. These large clusters have, on average, higher deformability which decreases the stability of force chains, promoting the loss of strength of the material.

The proposed 3D approach respects another essential feature of loops: they form a partition of the sample domain (i.e. the sum of the volume of the clusters is equal to the total volume). Consequently, the given definition of clusters enables the derivation of macroscopic quantities as the volume average of mesoscale ones.

As for future investigations, pursuing the 3D extensions of all known loop characteristics will be interesting. In particular, the co-evolution of force chains, clusters, and shear band localization [2, 3, 6, 12, 33]. Furthermore, tracking clusters' lifespan and life expectancy, their anisotropy properties, and the void ratio will reveal the elementary mechanisms responsible for the complex behavior of granular materials in a 3D framework [4, 47, 48].

In developing micro-mechanical models for the constitutive behavior of materials, clusters of medium and lower categories could be used to encapsulate the granular physics at the mesoscale. This is probably the case for the 3D H-model proposed by Xiong et al. [49], in which the proposed mesostructure is a bi-hexagon, equivalent to a cluster of order 18 and size 10. It is probably worth exploring in detail the statistics of medium clusters from the perspective of proposing new micro-mechanical models and improving existing ones.

Finally, the space cell system [26] is the equivalent of a Delaunay tessellation for any convex-shaped particles. Thus an algorithm capable of identifying space cell systems, and consequently edges and surfaces, would allow the identification of loops and clusters structures for more complex granular shapes. Therefore, loop-like theories may be applied to materials that better represent reality.

Acknowledgments. This work is supported by public funding through a Ph.D. scholarship with the university INSA de Lyon.

Declarations

Conflict of interest: The authors declare no conflict of interest.

References

[1] Satake, M.: A discrete-mechanical approach to granular materials. International Journal of Engineering Science **30**(10), 1525–1533 (1992). https://doi.org/10.1016/0020-7225(92)90162-A

[2] Tordesillas, A., Walker, D.M., Lin, Q.: Force cycles and force chains. Physical Review E **81**(1), 011302 (2010). https://doi.org/10.1103/PhysRevE.81.011302

[3] Tordesillas, A., Steer, C.A.H., Walker, D.M.: Force chain and contact cycle evolution in a dense granular material under shallow penetration. Nonlinear Processes in Geophysics **21**(2), 505–519 (2014). https://doi.org/10.5194/npg-21-505-2014

[4] Kruyt, N.P., Rothenburg, L.: On micromechanical characteristics of the critical state of two-dimensional granular materials. Acta Mechanica **225**(8), 2301–2318 (2014). https://doi.org/10.1007/s00707-014-1128-y

[5] Zhu, H., Nicot, F., Darve, F.: Meso-structure evolution in a 2D granular material during biaxial loading. Granular Matter **18**(1), 3 (2016). https://doi.org/10.1007/s10035-016-0608-2

[6] Liu, J., Wautier, A., Bonelli, S., Nicot, F., Darve, F.: Macroscopic softening in granular materials from a mesoscale perspective. International Journal of Solids and Structures **193-194**, 222–238 (2020). https://doi.org/10.1016/j.ijsolstr.2020.02.022. Accessed 2022-07-20

[7] Sun, X., Kob, W., Blumenfeld, R., Tong, H., Wang, Y., Zhang, J.: Friction-Controlled Entropy-Stability Competition in Granular Systems. Physical Review Letters **125**(26), 268005 (2020). https://doi.org/10.1103/PhysRevLett.125.268005. Accessed 2023-02-08

[8] Wanjura, C.C., Gago, P., Matsushima, T., Blumenfeld, R.: Structural evolution of granular systems: theory. Granular Matter **22**(4) (2020). https://doi.org/10.1007/s10035-020-01056-4

[9] Blumenfeld, R.: Stress in planar cellular solids and isostatic granular assemblies: coarse-graining the constitutive equation. Physica A: Statistical Mechanics and its Applications **336**(3), 361–368 (2004). https://doi.org/10.1016/j.physa.2003.12.043

[10] Peters, J.F., Muthuswamy, M., Wibowo, J., Tordesillas, A.: Characterization of force chains in granular material. Physical Review E **72**(4), 041307 (2005). https://doi.org/10.1103/PhysRevE.72.041307

[11] Sun, Q., Jin, F., Liu, J., Zhang, G.: Understanding force chain in dense granular materials. International Journal of Modern Physics B **24**(29), 5743–5759 (2010). https://doi.org/10.1142/S0217979210055780

[12] Zhu, H., Nicot, F., Darve, F.: Meso-structure organization in two-dimensional granular materials along biaxial loading path. International Journal of Solids and Structures **96**, 25–37 (2016). https://doi.org/10.1016/j.ijsolstr.2016.06.025

[13] Alshibli, K.A., El-Saidany, H.A.: Quantifying Void Ratio in Granular Materials Using Voronoi Tessellation. Journal of Computing in Civil Engineering **15**(3), 232–238 (2001). https://doi.org/10.1061/(ASCE)0887-3801(2001)15:3(232)

[14] Al-Raoush, R., Thompson, K., Willson, C.S.: Comparison of Network Generation Techniques for Unconsolidated Porous Media. Soil Science Society of America Journal **67**(6), 1687–1700 (2003). https://doi.org/10.2136/sssaj2003.1687

[15] Reboul, N., Vincens, E., Cambou, B.: A statistical analysis of void size distribution in a simulated narrowly graded packing of spheres. Granular Matter **10**(6), 457–468 (2008). https://doi.org/10.1007/s10035-008-0111-5

[16] O'Sullivan, C., Bluthé, J., Sejpar, K., Shire, T., Cheung, L.Y.G.: Contact based void partitioning to assess filtration properties in DEM simulations. Computers and Geotechnics **64**, 120–131 (2015). https://doi.org/10.1016/j.compgeo.2014.11.003

[17] Nguyen, N.-S., Taha, H., Marot, D.: A new Delaunay triangulation-based approach to characterize the pore network in granular materials. Acta Geotechnica (2021). https://doi.org/10.1007/s11440-021-01157-1

[18] Nicot, F., Darve, F.: The H-microdirectional model: Accounting for a mesoscopic scale. Mechanics of Materials **43**(12), 918–929 (2011). https://doi.org/10.1016/j.mechmat.2011.07.006

[19] Love, A.E.H.: A Treatise on the Mathematical Theory of Elasticity. Cambridge university press, Cambridge (1927)

[20] Weber, J.: Recherches concernant les contraintes intergranulaires dans lesmilieux pulvérulents. Bulletin de Liaison des Ponts-et-Chaussées **20**, 1–20 (1966)

[21] Bathurst, R.J., Rothenburg, L.: Observations

on stress-force-favbric relationship in idealized granular materials. Mechanics of Materials **9**(1), 65–80 (1989). https://doi.org/10.1016/0167-6636(90)90030-J

[22] Bagi, K.: On the definition of stress and strain in granular assemblies through the relation between micro-and macro-level characteristics. Powders & grains **93**, 117–121 (1993)

[23] Radjai, F., Wolf, D.E., Jean, M., Moreau, J.-J.: Bimodal Character of Stress Transmission in Granular Packings. Physical Review Letters **80**(1), 61–64 (1998). https://doi.org/10.1103/PhysRevLett.80.61

[24] Satake, M.: Tensorial form definitions of discrete-mechanical quantities for granular assemblies. International Journal of Solids and Structures **41**(21), 5775–5791 (2004). https://doi.org/10.1016/j.ijsolstr.2004.05.046

[25] Nguyen, N.-S., Magoariec, H., Cambou, B.: Local stress analysis in granular materials at a mesoscale. International Journal for Numerical and Analytical Methods in Geomechanics **36**(14), 1609–1635 (2012). https://doi.org/10.1002/nag.1063

[26] Bagi, K.: Stress and strain in granular assemblies. Mechanics of Materials **22**(3), 165–177 (1996). https://doi.org/10.1016/0167-6636(95)00044-5

[27] Kruyt, N., Rothenburg, L.: Micromechanical definition of the strain tensor for granular materials. J. Appl. Mech. (1996). https://doi.org/10.1115/1.2823353. ASME

[28] Cambou, B., Chaze, M., Dedecker, F.: Change of scale in granular materials. European Journal of Mechanics - A/Solids **19**(6), 999–1014 (2000). https://doi.org/10.1016/S0997-7538(00)01114-1

[29] Ball, R.C., Blumenfeld, R.: Stress Field in Granular Systems: Loop Forces and Potential Formulation. Phys. Rev. Lett. **88**(11), 115505 (2002). https://doi.org/10.1103/PhysRevLett.88.115505. Publisher: American Physical Society

[30] Kruyt, N.P.: Statics and kinematics of discrete Cosserat-type granular materials. International Journal of Solids and Structures **40**(3), 511–534 (2003). https://doi.org/10.1016/S0020-7683(02)00624-8

[31] Nicot, F., Hadda, N., Guessasma, M., Fortin, J., Millet, O.: On the definition of the stress tensor in granular media. International Journal of Solids and Structures **50**(14-15), 2508–2517 (2013). https://doi.org/10.1016/j.ijsolstr.2013.04.001

[32] Oda, M., Kazama, H., Konishi, J.: Effects of induced anisotropy on the development of shear bands in granular materials. Mechanics of Materials **28**(1-4), 103–111 (1998). https://doi.org/10.1016/S0167-6636(97)00018-5. Accessed 2021-01-11

[33] Liu, J., Nicot, F., Zhou, W.: Sustainability of internal structures during shear band forming in 2D granular materials. Powder Technology **338**, 458–470 (2018). https://doi.org/10.1016/j.powtec.2018.07.001

[34] Nguyen, N., Magoariec, H., Vincens, E., Cambou, B.: On the definition of a relevant meso-scale for upscaling the mechanical behavior of 3D granular materials. Granular Matter (2020). https://doi.org/10.1007/s10035-019-0972-9. SPRINGER

[35] Reboul, N., Vincens, E., Cambou, B.: A computational procedure to assess the distribution of constriction sizes for an assembly of spheres. Computers and Geotechnics **37**(1-2), 195–206 (2010). https://doi.org/10.1016/j.compgeo.2009.09.002

[36] Gao, S., Meegoda, J.N., Hu, L.: Two methods for pore network of porous media. International Journal for Numerical and Analytical Methods in Geomechanics **36**(18), 1954–1970 (2012). https://doi.org/10.1002/nag.1134

[37] Kang, D.H., Choo, J., Yun, T.S.: Evolution of pore characteristics in the 3D numerical direct shear test. Computers and Geotechnics **49**, 53–61 (2013). https://doi.org/10.1016/j.compgeo.2012.10.009

[38] Sufian, A., Russell, A.R., Whittle, A.J., Saadatfar, M.: Pore shapes, volume distribution and orientations in monodisperse granular assemblies. Granular Matter **17**(6), 727–742 (2015). https://doi.org/10.1007/s10035-015-0590-0

[39] Kuhn, M.R., Daouadji, A.: Multi-directional behavior of granular materials and its relation to incremental elasto-plasticity. International Journal of Solids and Structures **152-153**, 305–323 (2018). https://doi.org/10.1016/j.ijsolstr.2018.07.005

[40] Sufian, A., Russell, A.R., Whittle, A.J.: Evolving pore orientation, shape and size in sheared granular assemblies. Granular Matter **21**(1), 4 (2019). https://doi.org/10.1007/s10035-018-0856-4

[41] Mellor, D.W.: Random close packing (RCP) of equal spheres: structure and implications for use as a model porous medium (1989). https://doi.org/10.21954/OU.RO.0000DFC0. Publisher: The Open University

[42] Blumenfeld, R., Edwards, S.F.: Granular Entropy: Explicit Calculations for Planar Assemblies. Physical Review Letters **90**(11), 114303 (2003). https://doi.org/10.1103/PhysRevLett.90.114303. Accessed 2023-02-08

[43] Kloss, C., Goniva, C., Hager, A., Amberger, S., Pirker, S.: Models, algorithms and validation for opensource DEM and CFD-DEM. Progress in Computational Fluid Dynamics, An International Journal **12**(2/3), 140 (2012). https://doi.org/10.1504/PCFD.2012.047457

[44] Christoffersen, J., Mehrabadi, M.M., Nemat-Nasser, S.: A Micromechanical Description of Granular Material Behavior. Journal of Applied Mechanics **48**(2), 339–344 (1981). https://doi.org/10.1115/1.3157619

[45] Mehrabadi, M.M., Nemat-Nasser, S., Oda, M.: On statistical description of stress and fabric in granular materials. International Journal for Numerical and Analytical Methods in Geomechanics **6**(1), 95–108 (1982). https://doi.org/10.1002/nag.1610060107

[46] de Saxcé, G., Fortin, J., Millet, O.: About the numerical simulation of the dynamics of granular media and the definition of the mean stress tensor. Mechanics of Materials **36**(12), 1175–1184 (2004). https://doi.org/10.1016/j.mechmat.2003.01.002

[47] Sufian, A., Russell, A.R., Whittle, A.J.: Anisotropy of contact networks in granular media and its influence on mobilised internal friction. Géotechnique, 1–14 (2017). https://doi.org/10.1680/jgeot.16.P.170

[48] Deng, N., Wautier, A., Tordesillas, A., Thiery, Y., Yin, Z.-Y., Hicher, P.-Y., Nicot, F.: Lifespan dynamics of cluster conformations in stationary regimes in granular materials. Physical Review E **105**(1), 014902 (2022). https://doi.org/10.1103/PhysRevE.105.014902. Accessed 2023-01-27

[49] Xiong, H., Nicot, F., Yin, Z.Y.: A three-dimensional micromechanically based model:. International Journal for Numerical and Analytical Methods in Geomechanics **41**(17), 1669–1686 (2017). https://doi.org/10.1002/nag.2692